NEOPLASIA
www.neoplasia.com

Volume 21 Number 2 February 2019 pp. 159–171 159

An Intratumor Pharmacokinetic/Pharmacodynamic Model for the Hypoxia-Activated Prodrug Evofosfamide (TH-302): Monotherapy Activity is Not Dependent on a Bystander Effect[1,2]

Cho Rong Hong[*], **William R. Wilson**[*,†] **and Kevin O. Hicks**[*,†]

[*]Auckland Cancer Society Research Centre, University of Auckland, Auckland, New Zealand; [†]Maurice Wilkins Centre, University of Auckland, Auckland, New Zealand

Abstract

Tumor hypoxia contributes to resistance to anticancer therapies. Hypoxia-activated prodrugs (HAPs) selectively target hypoxic cells and their activity can extend to well-oxygenated areas of tumors via diffusion of active metabolites. This type of bystander effect has been suggested to be responsible for the single agent activity of the clinical-stage HAP evofosfamide (TH-302) but direct evidence is lacking. To dissect the contribution of bystander effects to TH-302 activity, we implemented a Green's function pharmacokinetic (PK) model to simulate the spatial distribution of O_2, TH-302 and its cytotoxic metabolites, bromo-isophosphoramide mustard (Br-IPM) and its dichloro derivative isophosphoramide mustard (IPM), in two digitized tumor microvascular networks. The model was parameterized from literature and experimentally, including measurement of diffusion coefficients of TH-302 and its metabolites in multicellular layer cultures. The latter studies demonstrate that Br-IPM and IPM cannot diffuse significantly from the cells in which they are generated, although evidence was obtained for diffusion of the hydroxylamine metabolite of TH-302. The spatially resolved PK model was linked to a pharmacodynamic (PD) model that describes cell killing probability at each point in the tumor microregion as a function of Br-IPM and IPM exposure. The resulting PK/PD model accurately predicted previously reported monotherapy activity of TH-302 in H460 tumors, without invoking a bystander effect, demonstrating that the notable single agent activity of TH-302 in tumors can be accounted for by significant bioreductive activation of TH-302 even in oxic regions, driven by the high plasma concentrations achievable with this well-tolerated prodrug.

Neoplasia (2019) 21, 159–171

Introduction

Tumor hypoxia promotes tumor progression and resistance to anticancer therapies through multiple mechanisms [1–5] and patients with more hypoxic tumors demonstrate a poor prognosis in several clinical settings [6–9]. Thus hypoxia-activated prodrugs (HAPs) can potentially improve clinical outcomes by killing hypoxic cells selectively [4,10–12], but utility of such agents is expected to be improved if active metabolites can diffuse to kill nearby cells. The resulting "bystander effect" has potential to ameliorate intratumoral heterogeneity of hypoxia and expression of prodrug activating reductases [13–15], and to facilitate both single agent activity of HAPs [16,17] and their use in combination with agents

Abbreviations: HAP, Hypoxia-activated prodrug; SR-PK/PD, Spatially resolved pharmacokinetic/pharmacodynamics; MCL, multicellular layers; AUC, Area under the concentration-time curve

Address all correspondence to: Dr Kevin O. Hicks, Auckland Cancer Society Research Centre, University of Auckland, 85 Park Rd, Grafton, Auckland 1023, New Zealand.

[1] Funding: This research was supported by a grant from Health Research Council of New Zealand (14/538), and a Cancer Society of New Zealand Training Scholarship to CR Hong.[2] Conflicts of interest: None.Received 6 September 2018; Revised 21 November 2018; Accepted 26 November 2018

1476-5586
https://doi.org/10.1016/j.neo.2018.11.009

that may not have exactly complementary oxygen dependencies [18,19].

Evofosfamide (TH-302), a prodrug of the DNA crosslinking agent bromo-isophosphoramide mustard (Br-IPM), has demonstrated promising results in early clinical trials [20–22] and has substantial activity in preclinical models [23–27]. TH-302 was originally suggested to be activated by reduction to the corresponding hydroxylamine via an O_2-sensitive nitro radical, with subsequent elimination of Br-IPM [28], but the nitro radical itself has subsequently been shown to fragment to generate Br-IPM [29,30] (Figure 1*A*). A bystander effect mediated by diffusion of Br-IPM has been suggested to play an important role in antitumor activity in xenograft models [23,26,31]. Evidence for a

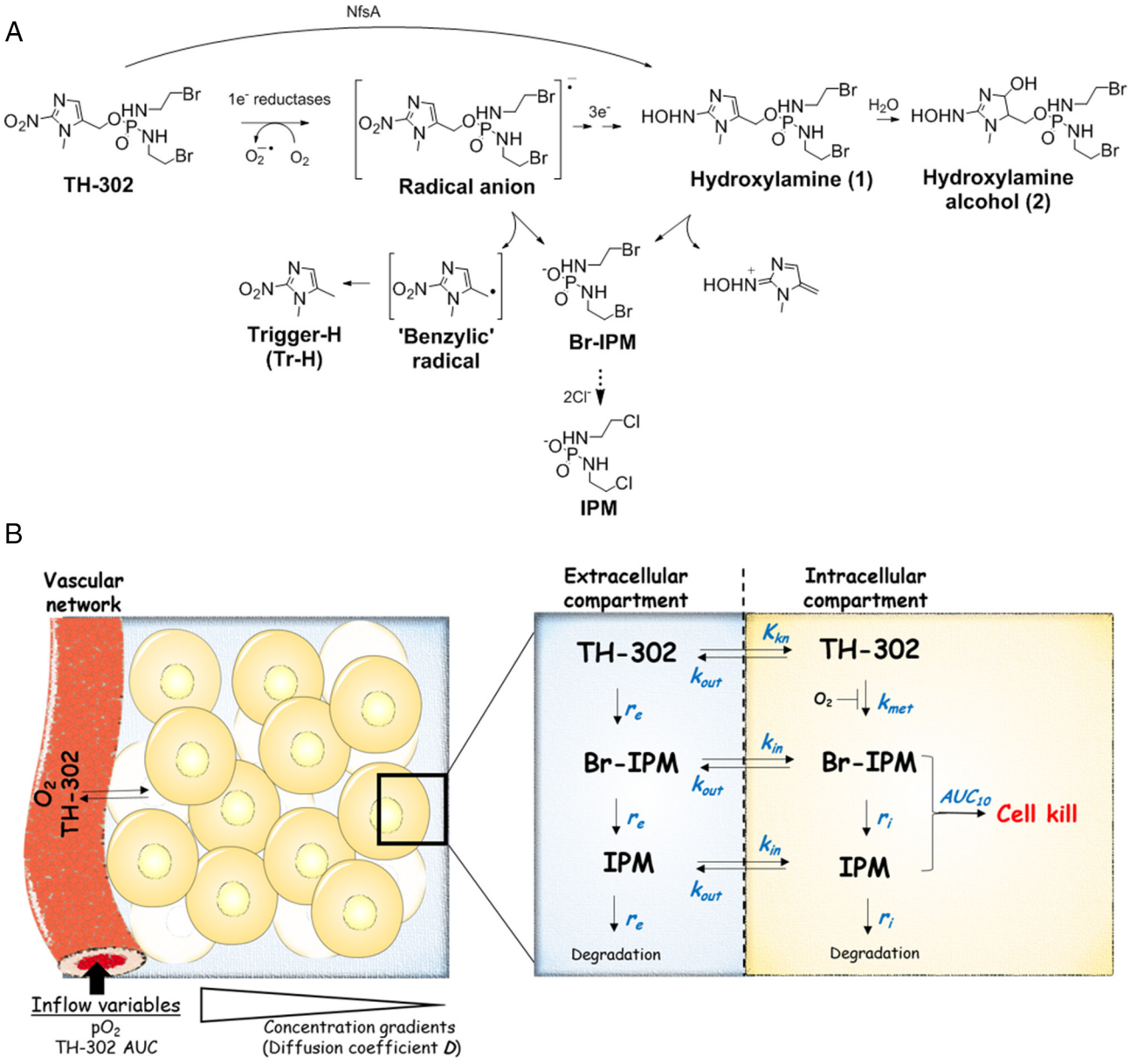

Figure 1. Schematic representation of activation pathway of TH-302 and the spatially resolved (SR)-PK/PD model. (A) Mechanism of TH-302 activation. 1-electron reduction of TH-302 generates a prodrug radical anion which further undergoes fragmentation to the DNA crosslinker Br-IPM and a benzylic radical (which generates 'Trigger-H'; Tr-H) under hypoxia. IPM is a more stable downstream product of Br-IPM that retains DNA crosslinking ability. In the presence of oxygen, the radical anion is rapidly back-oxidized to the parent prodrug, suppressing Br-IPM formation. In addition, under hypoxia the radical anion can be further reduced to the hydroxylamine (**1**), which can also fragment to Br-IPM. Hydration of the hydroxylamine generates the relatively stable hydroxylamine alcohol (**2**). The *E.coli* 2-electron nitroreductase NfsA bypasses formation of the radical anion and generates the hydroxylamine (**1**) even in the presence of O_2. (B) The SR-PK/PD model employs Green's functions to calculate steady-state concentration gradients of O_2, TH-302 and its metabolites in mapped microvascular networks. Blood flows are adjusted to simulate observed hypoxic fractions, and TH-302 inputs are defined by the measured plasma PK of TH-302 in mice. Diffusion of TH-302 and metabolites in the extracellular compartment is determined by their diffusion coefficients (*D*), while transport across the plasma membrane is defined by the rate constants k_{in} and k_{out}. Metabolic activation of TH-302 (rate constant k_{met}), as a function of O_2 concentration, is restricted to the intracellular compartment, whereas chemical reduction of TH-302 in extracellular compartment and extra- and intracellular formation of Br-IPM and IPM are defined by r_e and r_i. These reaction-transport parameters determine the AUC of the prodrug and its metabolites, and thus cell killing probability, at each point of the tumor microenvironment.

bystander effect includes antitumor activity greater than can be accounted for by killing of hypoxic cells (stained by pimonidazole) alone [26], and by a delayed γH2AX response in the oxic compartment [23,26]. However, this delay may reflect the requirement for cells with low levels of DNA crosslinks to progress into S-phase before γH2AX is detectable [32], rather than slow diffusion of a bystander effect mediator.

Although there is no direct evidence for a bystander effect from hypoxic activation of TH-302, Meng et al. [29] have demonstrated a bystander effect from TH-302 in multicellular layer (MCL) co-cultures comprising cells that express the oxygen insensitive *E. coli* nitroreductase NfsA under hyperoxic condition. However, we have shown that the metabolite profile from TH-302 reduction by NfsA, which is a two-electron reductase, is different from endogenous one-electron reductases in hypoxic tumor cells; NfsA further reduces the initial radical anion to a 4-electron reduction product (the hydroxylamine of TH-302, **1**) which can fragment to Br-IPM, whereas under hypoxia Br-IPM is generated predominantly from fragmentation of the initial nitro radical, with only the latter generating 1,5-dimethyl-2-nitroimidazole ("trigger-H"; Tr-H) (Figure 1*A*) [33]. Further to this, Br-IPM, which has been suggested to mediate bystander effects of TH-302, and its downstream product from bromine displacement by Cl ion (isophosphoramide mustard, IPM), are dramatically less cytotoxic when added to extracellular medium compared to when generated intracellularly from the prodrug because these hydrophilic metabolites (calculated $LogD_{7.4} < -2$) cannot diffuse across the plasma membrane efficiently [33]. These observations caused us to question whether there is a significant bystander effect following hypoxic activation of TH-302.

To evaluate whether a bystander effect is required to account for tumor cell killing by TH-302 outside the hypoxic subpopulation, here we deploy a spatially resolved pharmacokinetic/pharmacodynamic (SR-PK/PD) computational model analogous to those we previously used for HAPs such as tirapazamine analogues [34–36] and the dinitrobenzamide mustard PR-104 [18,37]. The steady-state spatial distributions of O_2, TH-302 and its metabolites in tissue regions defined by mapped microvascular networks [18,38] are simulated using Green's function solutions of the reaction–diffusion equations for each species (Figure 1*B*). Input concentrations from blood, and O_2 tissue transport (diffusion–reaction) parameters, are sourced from literature, while transport parameters for TH-302 and metabolites are determined experimentally by quantifying flux through multicellular layers (MCL) of HCT116 cells. MCLs are prepared by seeding tumor cells on permeable supports and grown to thicknesses of ~200 μm at which stage they are can be mounted in diffusion chambers to provide a well-validated experimental model for quantifying extravascular drug transport [18,35,39–43]. The cellular PK/PD model, describing the probability of cell killing by TH-302 at each point in the tumor tissue microregions, is parameterized from measurements of TH-302 bioreductive metabolism and clonogenic cell killing in HCT116 cell monolayers. We use the model to simulate tumor cell killing in xenografts and compare the model output with reported clonogenic cell killing in H460 tumors under a range of respiratory O_2 concentrations [26], and to investigate whether the PK/PD parameters for TH-302 are optimal for a HAP of this nature.

Materials and Methods

Compounds

TH-302 and Br-IPM were gifts from Threshold Pharmaceuticals [29]. Tr-H and deuterated stable isotope internal standards of Tr-H (D_3-Tr-H) and Br-IPM (D_8-Br-IPM) were synthesized at Auckland Cancer Society Research Center (ACSRC) as reported [33]. All compounds were dissolved in DMSO and stock solutions were stored at −80 °C.

Cell Lines

The HCT116 colon carcinoma cell line, from ATCC, was authenticated by short tandem repeat profiling and maintained in log-phase monolayers in αMEM containing 5% FBS. HCT116 cells with a forced expression of NfsA (HCT116/NfsA) has been reported previously [44], and was grown in the same medium with 2 μM puromycin. Both lines were *Mycoplasma*-free by PlasmoTest (InvivoGen).

Multicellular layer (MCL) Diffusion Assay

MCLs were cultured by seeding HCT116 or HCT116/NfsA cells (10^6 cells) on collagen-coated porous Teflon support membranes in Millicell culture inserts (Merck Millipore), and growing submerged in stirred reservoirs of culture medium as previously [18] for 4 days. MCLs were equilibrated under hyperoxia (5% CO_2/95% O_2; to suppress central hypoxia [41]) or anoxia (5% CO_2/95% N_2) for 60 min in diffusion chambers (Figure 2*A*). TH-302 (30 μM) was added to the donor compartment with ^{3}H-mannitol (1 μM, 20 Ci/mmol, American Radiolabeled Chemicals Inc.) and ^{14}C-urea (1 μM, 2.11 GBq/mmol, Amersham) to assess the integrity and average thickness of MCLs, respectively [43]. Medium (100 μl) was sampled from the donor and receiver compartments at intervals for liquid scintillation counting and LC–MS/MS analysis of TH-302 and its metabolites. Extracellular medium was deproteinized with 2 volumes of ice-cold 80% methanol/20% water (v/v) with 0.5% formic acid containing 5 μM D_3-Tr-H and D_8-Br-IPM internal standards and stored at −80 °C prior to LC–MS/MS.

LC–MS/MS Assay for Quantitation of TH-302 and Its Metabolites

Methanol extracts were centrifuged (13,000 g for 5 min at 4 °C) and analyzed with an Agilent LC–MS/MS (model 6460) using a Jet Stream Electrospray Ionization Source (ESI) and photodiode array absorbance detector with a Phenomenex Synergi column (100 × 3.00 mm, 2.5 μm Polar, RP-10A). TH-302, Tr-H, Br-IPM and IPM were quantified using multiple reaction monitoring (MRM) as previously reported [33].

Reaction–Diffusion Modeling

The PK/PD model for TH-302 and its products follows the scheme in Figure 1*B* using a 2-compartment model for each compound. Concentrations in the extracellular (C_e) and intracellular (C_i) compartments for each species (TH-302, Br-IPM, IPM and an intermediate (INT) between Br-IPM and IPM; kinetics shown in Supplementary Methods) were calculated as follows:

$$\varphi_e \frac{\partial C_e}{\partial t} = D\nabla^2 C_e - \varphi_i(k_{in}C_e - k_{out}C_i) - \varphi_e r_e C_e + \varphi_e r_{e(-1)} C_{e(-1)} \quad (1)$$

$$\left.\begin{aligned} \varphi_i \frac{\partial C_i}{\partial t} &= \varphi_i(k_{in}C_e - k_{out}C_i) - \varphi_i k_{met} C_i \text{ for TH-302} \\ \varphi_i \frac{\partial C_i}{\partial t} &= \varphi_i(k_{in}C_e - k_{out}C_i) - \varphi_i r_i C_i + \varphi_i r_{i(-1)} C_{i(-1)} \text{ for metabolites} \end{aligned}\right\} \quad (2)$$

Diffusion is assumed to occur extracellularly, with diffusion coefficient D. φ_i and φ_e are the intra- and extracellular volume

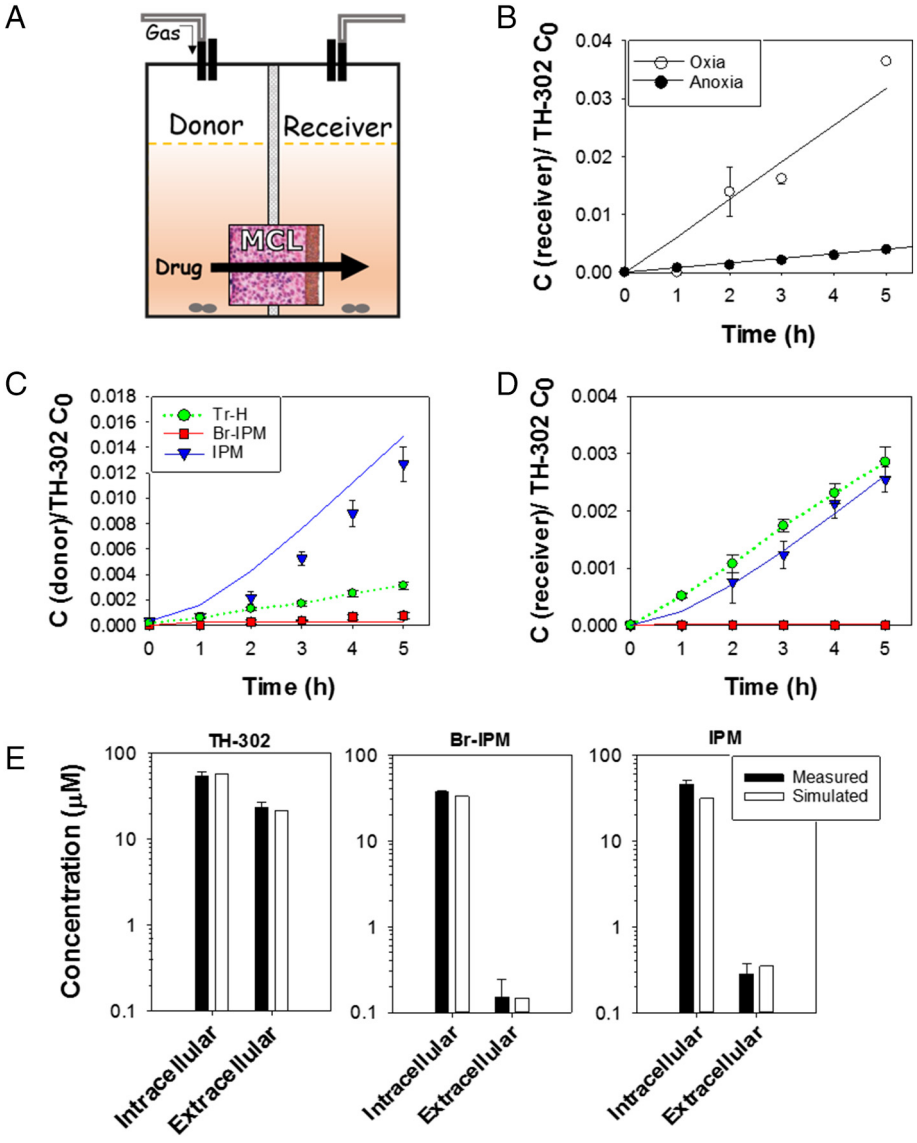

Figure 2. Transport of TH-302 and its metabolites through HCT116 multicellular layers (MCLs). (A) Diagram of MCL flux apparatus. An MCL is inserted between the donor and receiver compartments and prodrug is added to the donor side. Concentrations of the prodrug and its metabolites are measured in both compartments at intervals. (B-D) Transport of TH-302 and its metabolites when 30 μM TH-302 was added to the donor. (B) Concentrations of TH-302 in the receiver compartment under hyperoxic or anoxic conditions, normalized to the initial concentration in the donor, C_0. (C,D) Concentrations of Tr-H, Br-IPM and IPM under anoxic conditions in the donor (C) and receiver (D) compartments. Mean and SE are from 3 MCLs, with estimated thicknesses (mean ± SE) of 139 ± 2 μm based on ^{14}C-urea flux. Solid lines are simulated concentrations for the diffusion–reaction model. (E) Predicted and measured intracellular and extracellular concentrations of TH-302, Br-IPM and IPM in monolayer cultures of HCT116 cells (10^6 cells/ 0.5 mL) when exposed to 30 μM TH-302 under anoxia. Measured values are from [33].

fractions with $\varphi_e = 1\text{-}\varphi_i$, ∇^2 is the Laplacian operator, k_{met} is the (oxygen-sensitive) rate constant for intracellular bioreductive metabolism of TH-302, k_{in} and k_{out} are rate constants for transfer between the intracellular and extracellular compartments and r_e and r_i are rate constants of extracellular or intracellular production of the current species from the previous species (indicated by (–1) subscript) in the pathway by spontaneous chemical reaction: chemical reduction of TH-302 to Br-IPM (extracellular compartment, only under anoxia), formation of (extracellular and intracellular) INT from Br-IPM, and IPM from INT respectively. Further details of modeling and parameter estimation are provided in Supplementary Methods.

SR-PK/PD Model

Green's function methods [38] were used to solve Eqs. (1) and (2) to simulate the steady-state concentration gradients of O_2, TH-302, Br-IPM and IPM in previously mapped microvascular networks from a R3230Ac rat mammary carcinoma [38] and a FaDu head and neck squamous cell carcinoma xenograft [45] grown in window chambers. Inflow of O_2 to the tumor microvascular network was adjusted to match the previously reported hypoxic fractions in HCT116 [18] and H460 tumors [26]. TH-302 inputs were defined by the area under the concentration-time curve (AUC) of TH-302 in plasma of nude mice [46] which provided a time-independent exposure variable.

Oxygen dependence of the rate constant for TH-302 metabolism, k_{met}, was introduced as:

$$k_{met} = \frac{K_{O_2}}{K_{O_2} + [O_2]} \; k_{met,0} \quad (3)$$

where $k_{met,\ 0}$ is the maximum rate constant, which occurs under anoxia and K_{O2} is the O_2 concentration for half-maximal rate of TH-302 metabolism.

The surviving fraction (SF) at each point of the tumor microregion was calculated from intracellular AUC of Br-IPM and IPM to account for bystander effects ('bystander' model).

$$\text{Log } cell\ kill = -\log_{10} SF = \frac{AUC\ metabolites}{AUC_{10}\ metabolites} \quad (4)$$

where AUC_{10}, the intracellular AUC required for 10% clonogenic survival, was estimated from clonogenic assays in monolayers. To turn off cell killing by bystander effects ('no bystander' model), SF was calculated from intracellular TH-302 AUC and its oxygen-sensitive rate of reductive metabolism, thus confining killing to the cells in which prodrug activation occurs:

$$\text{Log } cell\ kill = -\log_{10} SF = \frac{K_{O_2}}{K_{O_2} + [O_2]} \; \frac{AUC\ TH302}{AUC_{10}\ TH302} \quad (5)$$

Results

Transport of TH-302 and Its Metabolites Through HCT116 MCLs

To investigate the extravascular transport characteristics of TH-302 and its metabolites MCLs were inserted between the donor and receiver compartments in diffusion chambers, drug was added to the donor side and drug concentrations were measured in both compartments at intervals (Figure 2*A*). First, we investigated transport of TH-302 through HCT116 MCLs under hyperoxic (95% O_2; to suppress central hypoxia in MCLs [41]) and anoxic conditions, monitoring concentrations of the prodrug and its major metabolites (Tr-H, Br-IPM and IPM). Concentrations of TH-302 were markedly lower in the receiver compartment under anoxia compared to hyperoxia (Figure 2*B*), indicating that metabolic consumption of TH-302 compromised its diffusion through anoxic MCLs. This interpretation was supported by the high concentrations of Tr-H, a non-cytotoxic [33] marker of the one-electron reduction pathway (Figure 1*A*), in the donor and receiver compartments under anoxia (Figure 2, *C* and *D*), while there was no detectable Tr-H or other TH-302 metabolites under hyperoxic conditions.

The detection of Tr-H in the donor and receiver compartments under anoxia (Figure 2, *C* and *D*) indicated that it diffuses across layers of cells readily. In contrast, Br-IPM was present at very low concentration in the donor compartment and was not detected in the receiver. Surprisingly, there were high concentrations of IPM in both donor and receiver compartments, apparently inconsistent with our previous observation that IPM is too hydrophilic to diffuse out of cells [33]. However, we found that the slow chemical reduction of TH-302 in anoxic medium that we previously reported [33] is responsible for this finding, as shown in Fig. S1.

The flux of TH-302 under hyperoxia (Figure 2*B*) was modeled to estimate the tissue (MCL) diffusion coefficient in the absence of metabolism, giving D = (1.82 ± 0.07) x 10^{-7} cm^2 s^{-1}. (All model parameters are listed in Table S1). The first order rate constant for TH-302 metabolism was determined from transport through anoxic HCT116 MCLs ($k_{met,0}$ = 0.0115 ± 0.05 s^{-1}), assuming an unchanged MCL diffusion coefficient. To describe transport across the plasma membrane, the rate constants k_{in} and k_{out} (Figure 1*B*) were fitted using measured steady-state intracellular and extracellular concentrations of TH-302, Br-IPM and IPM during metabolism of TH-302 by anoxic HCT116 monolayer cultures (Figure 2*E*). There was a ~100 fold difference in Br-IPM and IPM concentrations between intracellular and extracellular space which were consistent with fitted k_{in} and k_{out} values for Br-IPM (both 0.001 s^{-1}) and IPM (both 0.0005 s^{-1}). These values were strikingly lower than that of TH-302 (k_{in} 0.15 s^{-1}, k_{out} 0.05 s^{-1}), confirming very low flux of Br-IPM and IPM across the plasma membrane.

Transport of Br-IPM and IPM

To investigate transport of Br-IPM and IPM through MCLs more directly, Br-IPM was added to the donor side of HCT116 MCLs. Rapid decay of Br-IPM was observed with a concomitant increase in IPM in the donor compartment (Figure 3*A*). No Br-IPM was detected in the receiver compartment, whereas there was a steady increase in concentration of IPM (Figure 3*B*) with a lag consistent with the previous demonstration that the reaction proceeds via Br/Cl-IPM and aziridinyl intermediates [33].

The mass balance for IPM at later times (total approximately 850 nmol) was similar to the Br-IPM input (842 nmol) suggesting essentially quantitative conversion of Br-IPM to IPM, so the rate constant for this reaction in the extracellular space was set equal to the previously determined rate constant for instability (r_e) of Br-IPM in culture medium at 37 °C [33]. The rate constants for conversion of Br-IPM and IPM to downstream products in cells (r_i) were fitted to the measured intracellular concentrations in monolayer cultures (Figure 2*E*). To model the lag in IPM formation, a single notional intermediate (INT) was incorporated into the kinetic model (Supplementary Methods) assuming that its D, k_{in}, and k_{out} is the same as IPM. The rate constants for conversion of INT to IPM in extracellular and intracellular compartments were determined using the flux data in Figures 2, *C* and *D* and 3, *A* and *B* (values in Supplementary Methods). Fitting this reaction–diffusion model gave D for IPM = (1.33 ± 0.04) x 10^{-7} cm^2/s, similar to the extracellular marker mannitol [47] in HCT116 MCLs (D = (1.46 ± 0.02) x 10^{-7} cm^2/s) and thus consistent with paracellular (extracellular) diffusion of IPM. Given the close physicochemical similarity of Br-IPM and IPM, and their similar retention by cells (Figure 2*E*), we assume the same D value for Br-IPM. Using the above reaction–diffusion parameters, the model showed good agreement with experimental results in MCLs (solid lines in Figures 2*B-D* and 3*A,B*).

Transport of Hydroxylamine Metabolites

The above observations suggest that Br-IPM and IPM are unlikely to be bystander mediators. We previously noted that products consistent with the hydroxylamino derivative of TH-302 (cmpd **1**) and its hydration product (cmpd **2**) can be detected at low levels in anoxic HCT116 cells by mass spectrometry, and at higher concentrations in HCT116 cells with forced expression of NfsA under either hyperoxia or anoxia [33]. We used HCT116/NfsA cells to generate higher levels of these products to investigate their diffusion. Diffusion of the ^{14}C-urea internal standard [43] was faster

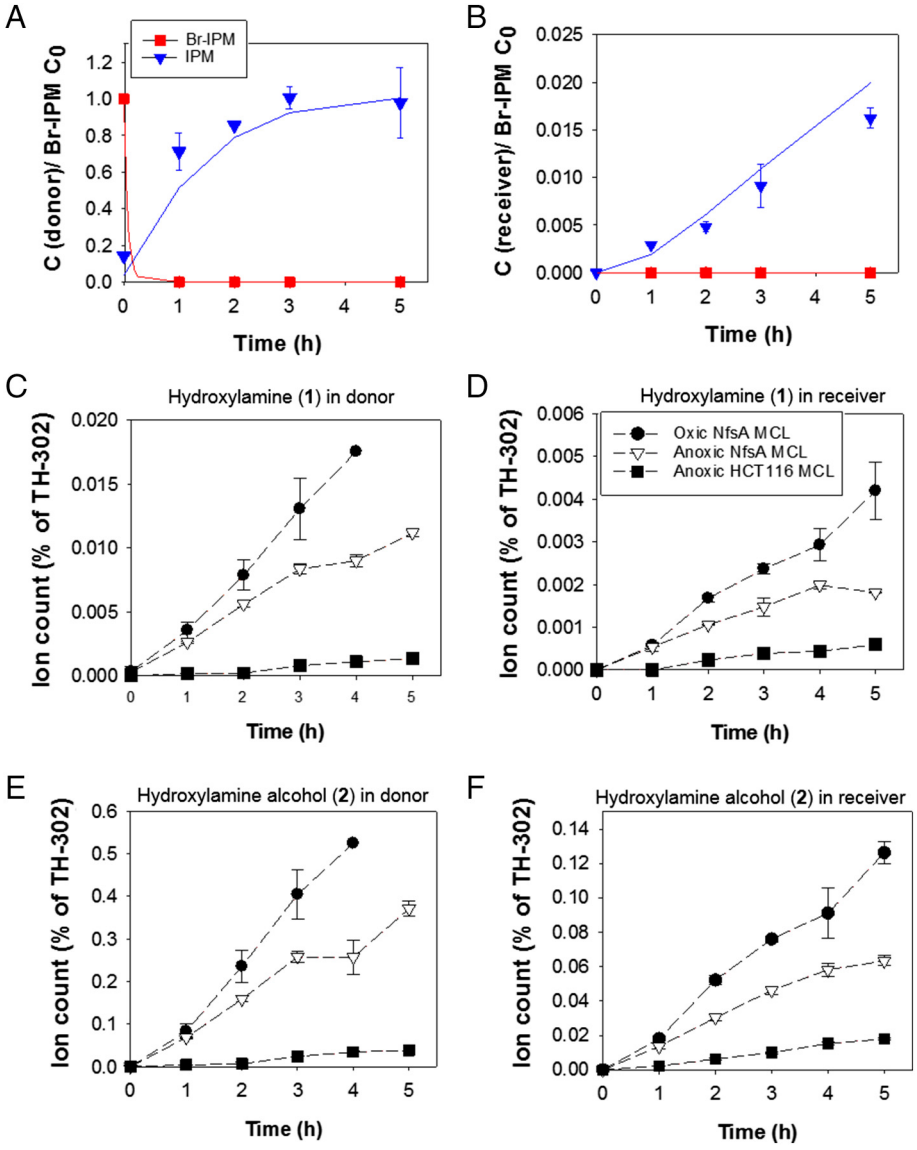

Figure 3. Transport of Br-IPM and IPM when Br-IPM in hyperoxic HCT116 MCLs and flux of the hydroxylamine (**1**) and hydroxylamine alcohol (**2**) in hyperoxic and anoxic HCT116/NfsA MCLs and anoxic HCT116 MCLs. (A,B) Concentrations of Br-IPM and IPM in the donor (A) and receiver (B) compartments when 100 μM Br-IPM was added to the donor side of hyperoxic HCT116 MCLs. Concentrations are normalized to the initial concentration of Br-IPM in the donor compartment, C_0. Mean and SE are from 3 MCLs, with estimated thicknesses of 122 ± 6 μm. Solid lines are simulated concentrations from the diffusion–reaction model described in the main text. (C-F) Ion counts of the hydroxylamine **1** (C,D) and the hydroxylamine alcohol **2** (E,F) in the donor (C,E) and the receiver (D,F) compartments based on the m/z 436 → 126 and m/z 454 → 126 transitions, respectively when 30 μM TH-302 was added to the donor side. Ion counts are % of initial ion counts of TH-302 in the donor. Mean and SE are estimates from 3 MCLs, with estimated thicknesses (mean and SE) of 139 ± 2, 113 ± 0 and 102 ± 1 μm for HCT116 anoxic, HCT116/NfsA anoxic and HCT116/NfsA hyperoxic MCLs, respectively.

through HCT116/NfsA MCLs than parental HCT116 MCLs (Fig. S2*A*). Correcting for this small difference in mean thickness of the MCLs, the flux of TH-302 through HCT116/NfsA MCLs under either anoxia or hyperoxia was slower than through parental HCT116 MCLs under anoxia (Fig. S2*B*), demonstrating a high rate of TH-302 reduction by NfsA expressed in these cells. This is consistent with higher concentrations of Br-IPM and IPM in HCT116/NfsA MCLs (Fig. S2*C*). Formation of Tr-H was partially suppressed in the NfsA MCLs under anoxia, and almost completely abolished under hyperoxia (Fig. S2*D*), confirming that reduction of TH-302 by NfsA bypasses the nitro radical anion (Figure 1*A*).

Notably, hydroxylamine **1** and its hydration product **2** could be detected by LC–MS/MS as TH-302 metabolites in both the donor (Figure 3*C*) and receiver (Figure 3*D*) compartments, at concentrations that increased in the order: anoxic HCT116 < anoxic HCT116/NfsA < hyperoxic HCT116/NfsA. A similar pattern was observed for the corresponding hydration product **2** (Figure 3, *E* and *F*). In the absence of authentic standards it was not possible to quantify these products, and interpretation is also complicated by differences in mean thickness in the three groups of MCLs as assessed by urea diffusion (Fig. S2*A*). However, anoxia lowered the concentrations of cmpds **1** and **2** from HCT116/NfsA cells (Figure 3, *C–F*),

suggesting that fragmentation of the radical anion of TH-302 dominates over further reduction to the hydroxylamine under hypoxia. Despite this, the high ion counts for cmpd **2**, even without expression of NfsA, suggests some metabolism of TH-302 to hydroxylamine **1** in hypoxic cells and that this could diffuse to release Br-IPM in nearby cells.

SR-PK/PD Modeling of TH-302 in HCT116 Tumors

To investigate the implications of the above diffusion and reaction properties of TH-302 and its metabolites for antitumor activity, we incorporated these PK parameters into a SR-PK/PD Green's function model to simulate concentrations of the prodrug and its metabolites at each point in tumor microregions which had been digitized in 3 dimensions and the vessel geometry, direction and velocity of blood flow and perivascular pO_2 have been measured accurately. One region (230 x 520 x 550 μm) is from a syngeneic rat R3230Ac mammary adenocarcinoma [38] and the other (990 x 810 x 150 μm) is from a FaDu head and neck squamous cell carcinoma xenograft [45]. These two networks are representative of the disorganized tumor microvasculature and heterogeneous oxygen distribution of xenografts [18,19,34,35,37].

TH-302 activation has been reported to be suppressed at lower O_2 concentration than required to inhibit tirapazamine [29] but K_{O2} for TH-302 is not precisely defined. For simulations, we used a K_{O2} value of 0.2 mmHg (0.27 μM, lower than the measured K_{O2} for tirapazamine of 1.3 μM, [37]) calculated from the previously reported hypoxia cytotoxicity ratio of TH-302 in HCT116 cells [33] assuming no oxygen-independent activation and no cytotoxicity of the unreduced prodrug as explained in Supplementary Methods. Inflow O_2 concentration was adjusted to match the previously reported hypoxic fraction (23%, defined as <1 μM O_2) measured by pimonidazole staining in HCT116 tumors [18] along with well-accepted O_2 transport parameters (Table S2). The previously reported plasma AUC of TH-302 (25 μM.h in nude mice following i.v. TH-302 at 50 mg/kg) [46] was used to define the input in all inflowing vessels of the tumor microregions. Given that Green's function models are steady-state descriptions of concentration profiles, the intermediates in the conversion of Br-IPM to IPM were treated as identical to IPM (they are all expected to be DNA crosslinkers with broadly similar properties) using measured r_e of Br-IPM [33] to describe direct conversion of Br-IPM to IPM (i.e. IPM in the Green's function model represents all the downstream metabolites from Br-IPM).

The SR-PK/PD simulations for this virtual HCT116 tumor based on the R3230Ac microvascular network demonstrated that intracellular concentrations of TH-302 are lowered in hypoxic regions, with a spatial distribution mirroring that of oxygen while the converse pattern was predicted for intracellular Br-IPM and IPM (Figure 4*A*). These distributions are quantified in Figure 4*B*, which displays AUC values and O_2 concentrations at each point in the microregion. Thus while metabolic consumption impedes penetration of TH-302, its metabolic activation to Br-IPM/IPM nonetheless mainly occurs in hypoxic regions as expected. Estimated extracellular concentrations of Br-IPM and IPM (Figure 4*C*) were markedly lower than inside cells as a result of cellular retention of these metabolites.

Clonogenic survival probability at each point in the tumor microregion was calculated from the intracellular AUC of Br-IPM and IPM, which accounts for any bystander effects resulting from diffusion of Br-IPM and IPM (the 'bystander' model; Eq. (4)). The PD parameter relating exposure to cell kill (AUC_{10}) was determined using monolayer clonogenic assay data (Fig. S3*A*), with Br-IPM and IPM assumed to be equally potent based on the observation that the apparent cytotoxic potency of Br-IPM in culture medium does not change as Br-IPM spontaneously converts to IPM [33]. To dissect the relative contribution of intracellular and diffusible metabolites to cell killing, the 'bystander' model was compared to a 'no bystander' model in which cell killing is a function of intracellular TH-302 AUC and its rate of metabolism (Eq. (5)), which has the effect of turning off any effect of diffusion of metabolites on cell killing. Estimation of AUC_{10} for this model is shown in Figure S3*B*.

The 'bystander' model predicted slightly higher killing throughout the tumor than the 'no bystander' model (Figure 4*D*). Averaging across whole tumor microregions (Figure 4*E*) showed that bystander effects mediated by Br-IPM and IPM cause only marginal increases in cell kill (corresponding to 6.4% cell survival without a bystander effect, versus 4.1% with a bystander effect). Averaging hypoxic (O_2< 1 μM) and oxic (O_2> 1 μM) regions also demonstrated little contribution from bystander effects (Figure 4*E*). Using the FaDu microvascular network (Fig. S4) gave similar predictions (Figure 4*F*), again with little contribution from Br-IPM/IPM bystander effects, although cell killing was higher in the hypoxic region than for the R3230Ac network as a result of shorter diffusion distances from vessels to hypoxic zones. The conclusion that Br-IPM/IPM bystander effects have little impact on the intratumor PK/PD of TH-302 was little affected by the assumed value of K_{O2} (Fig. S5).

Evaluation of the Model by Comparison with Single Agent Activity of TH-302 in H460 Tumors

We tested the SR-PK/PD model by comparing the model outputs, for the R3230Ac microvascular network, to previously reported monotherapy activity of TH-302 against H460 xenografts in mice breathing oxygen at 10, 21 or 95% [26]. The inflow of oxygen in air-breathing mice was adjusted to match the 16% hypoxic fraction measured by pimonidazole binding [26], while the effects of breathing 95% and 10% O_2 were simulated by modulating O_2 concentrations in the inflowing blood. The resulting O_2 concentration-distance relationships and hypoxic fractions are shown in Figure 5*A-C*. To model TH-302 activity we used the same PK/PD parameters as for HCT116 cells, given the very similar rate of TH-302 metabolism in anoxic H460 and HCT116 cells (Fig. S6) and their equivalent sensitivity to TH-302 when growth inhibition was measured 7 days after a 2 h anoxic exposure in vitro (IC_{50} 0.2 μM for both; personal communication, Dr. Charles Hart, Threshold Pharmaceuticals). The SR-PK/PD model predictions for these virtual H460 tumors were in good agreement with the experimental observations from Sun et al. [26], with increasing TH-302 activity as the ambient O_2 concentration decreases (Figure 5*D*); as for the HCT116 models there was only a minor contribution from a Br-IPM/IPM bystander effect (Figure 5*D*). Given that the hypoxia fraction in H460 tumors has been reported to be between 8–18% [26,48], simulation was repeated with higher oxygen input to simulate 10% hypoxia fraction but there was little difference in cell killing (data not shown), indicating that the model is fairly robust.

Understanding and Optimizing the Intratumor PK/PD of TH-302

We then used the SR-PK/PD model, with the H460 parameters and the R3230Ac microvascular network, to explore questions about the intratumor PK/PD of TH-302 that are not readily experimentally accessible. Br-IPM has been detected in plasma of patients treated with TH-302 with an AUC ~2% of TH-302 [20], and at higher

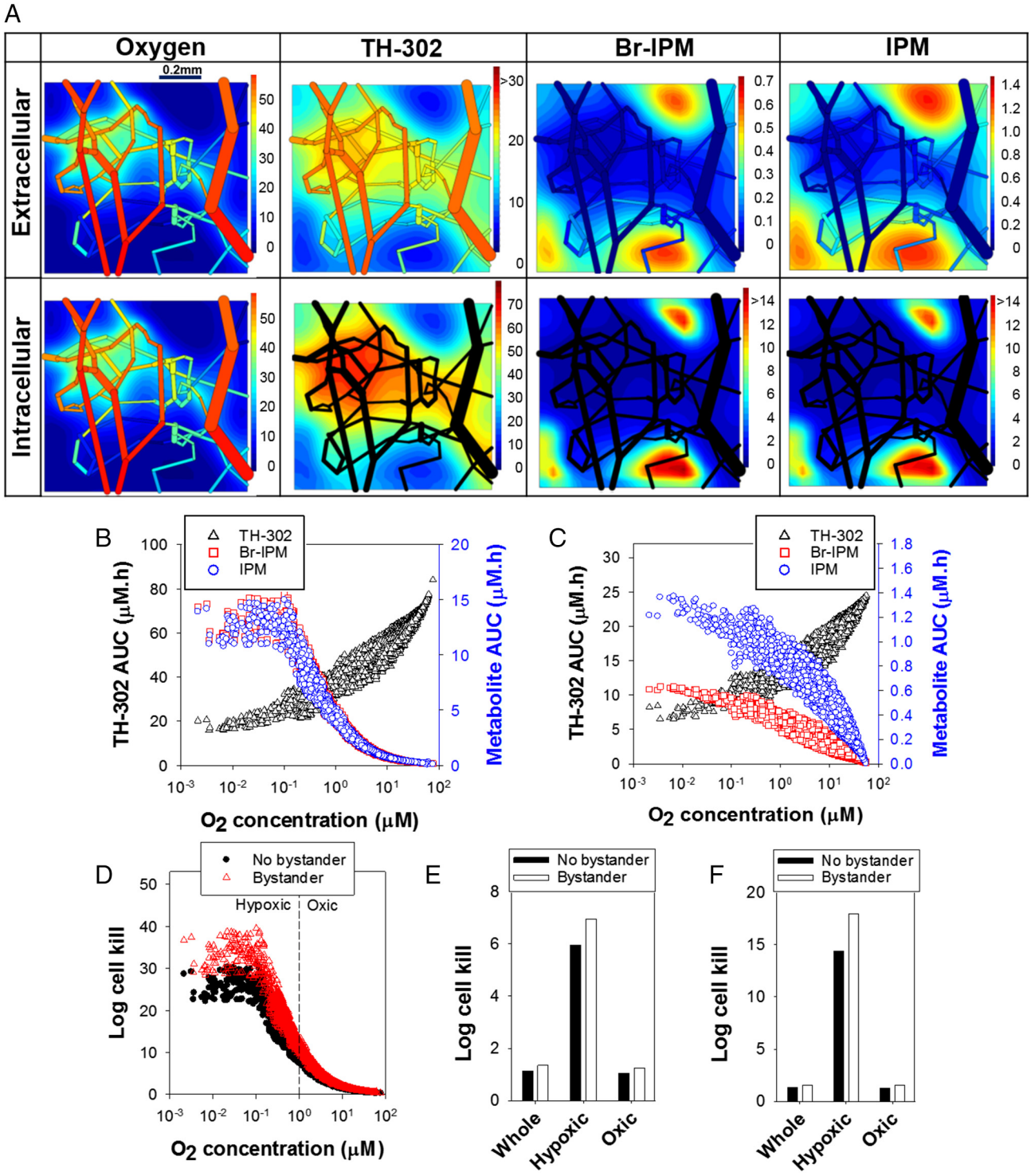

Figure 4. SR-PK/PD model predictions for a virtual HCT116 tumor following intravenous administration of 50 mg/kg of TH-302 (plasma AUC 25 μM.h) in nude mice. (A-E) Model predictions using a microvascular network from the R3230Ac breast adenocarcinoma (A) Contour plot of extracellular and steady state intracellular concentrations of O_2 (mmHg), and AUC values for TH-302, Br-IPM and IPM (μM.h) across the transverse section 100 μm into the z-plane of the tumor microregion, superimposed with the whole microvascular network projected onto the plane. Note the very different scales for the intracellular and extracellular metabolites. (B,C) Model predictions for intracellular (B) and extracellular (C) concentrations of TH-302, Br-IPM and IPM versus O_2 concentrations in the tumor microregion. (D) Predicted log cell kill by the 'no bystander' and 'bystander' models. (E,F) Predicted average log cell kill in the whole tumor microregion or hypoxic (O_2< 1 μM) and oxic (O_2> 1 μM) regions for the two models using the R3230Ac (E) or Fadu (F) microvascular networks.

levels (~10% of TH-302) in rats [46]. We investigated the contribution of systemic active metabolites to antitumor activity, under the assumptions that plasma AUC of IPM (not measured in the PK studies) is the same as Br-IPM at the higher level (10% of TH-302 AUC); assumed values are shown in Table S1. Addition of these systemic metabolites to the base model increased extracellular

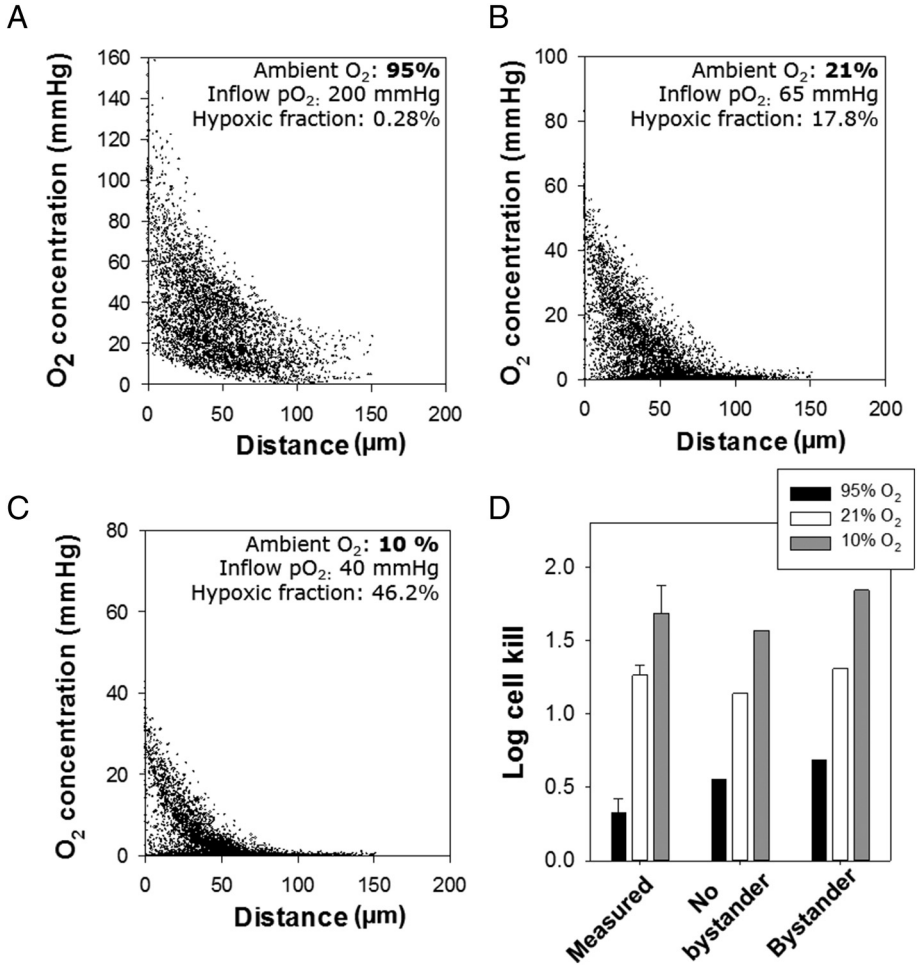

Figure 5. SR-PK/PD model predictions for activity of TH-302 in a virtual H460 tumor, using the R3230Ac microvascular network, in mice treated i.v. with 50 mg/kg of TH-302. (A-C) Simulated tissue O_2 concentrations in the tumor microregion for mice breathing 95% (A), 21% (B) or 10% O_2 (C). Inflow of O_2 (mmHg) in mice breathing 21% O_2 was adjusted to achieve a hypoxic fraction (< 1 μM) corresponding to the mean pimonidazole-positive fraction measured in H460 tumors [26]. Inflow of O_2 was adjusted to simulate O_2 concentrations in mice breathing 95% and 10% O_2. (D) Predicted average log cell kill for tumors in mice breathing O_2 at the three different concentrations. Measured log cell kill in H460 tumors from [26].

Br-IPM, especially near vessels, and IPM throughout the tumor (Figure 6*A*) but had little impact on intracellular concentrations (data not shown) or cell killing (Figure 6*B*) because of the low rates of their cellular uptake.

A further question amenable to examination with the SR-PK/PD model is whether the PK parameters of TH-302 are optimal for a HAP like TH-302 that generates hydrophilic reactive cytotoxic metabolites. We modulated the rate of reductive metabolism of the prodrug by varying $k_{met,0}$, demonstrating that penetration into hypoxic regions decreases as $k_{met,0}$ increases because of consumption in cells closer to blood vessels (Fig. S7). This resulted in increased killing of the most oxic cells but highly variable killing in cells at low O_2 depending on their position in the network (Figure 6*C*). As a result, predicted killing averaged over the whole virtual tumor increased monotonically with $k_{met,0}$ while killing of hypoxic cells was optimal at 0.042 s^{-1} (3.5-fold higher than the value for TH-302 in HCT116 MCLs) reflecting the opposing effects of prodrug metabolism on penetration and cytotoxic potency (Figure 6*D*).

Next we evaluated whether a more efficient bystander effect, resulting from increased membrane permeability of the active metabolites, would enhance hypoxia-dependent killing of oxic cells in tumors. Increasing membrane permeability by raising k_{in} and k_{out} of metabolites resulted in greater diffusion from hypoxic regions (Fig. S8) and increased killing in oxic regions while killing of hypoxic cells decreased (Figure 6*E*). However there was only a minor increase in single agent activity (Figure 6*F*) as permeability of metabolites increased washout into the vasculature which has been noted as a potential limitation with readily diffusible bystander mediators [19]. Of interest, metabolites with higher D as well as high k_{in} and k_{out} are predicted to be able to better exploit bystander effects to enhance monotherapy activity (Figure 6*F*).

Discussion

The central question addressed in this research is whether a hypoxia-mediated bystander effect is necessary to explain the observed single agent activity of TH-302 in tumor xenografts. This question has broader implications for the argument that HAPs that generate bystander metabolites will be needed to exploit tumor hypoxia optimally [12,16–19]. To clarify the intratumoral PK/PD of TH-302, we undertake the first measurements of the transport of TH-302

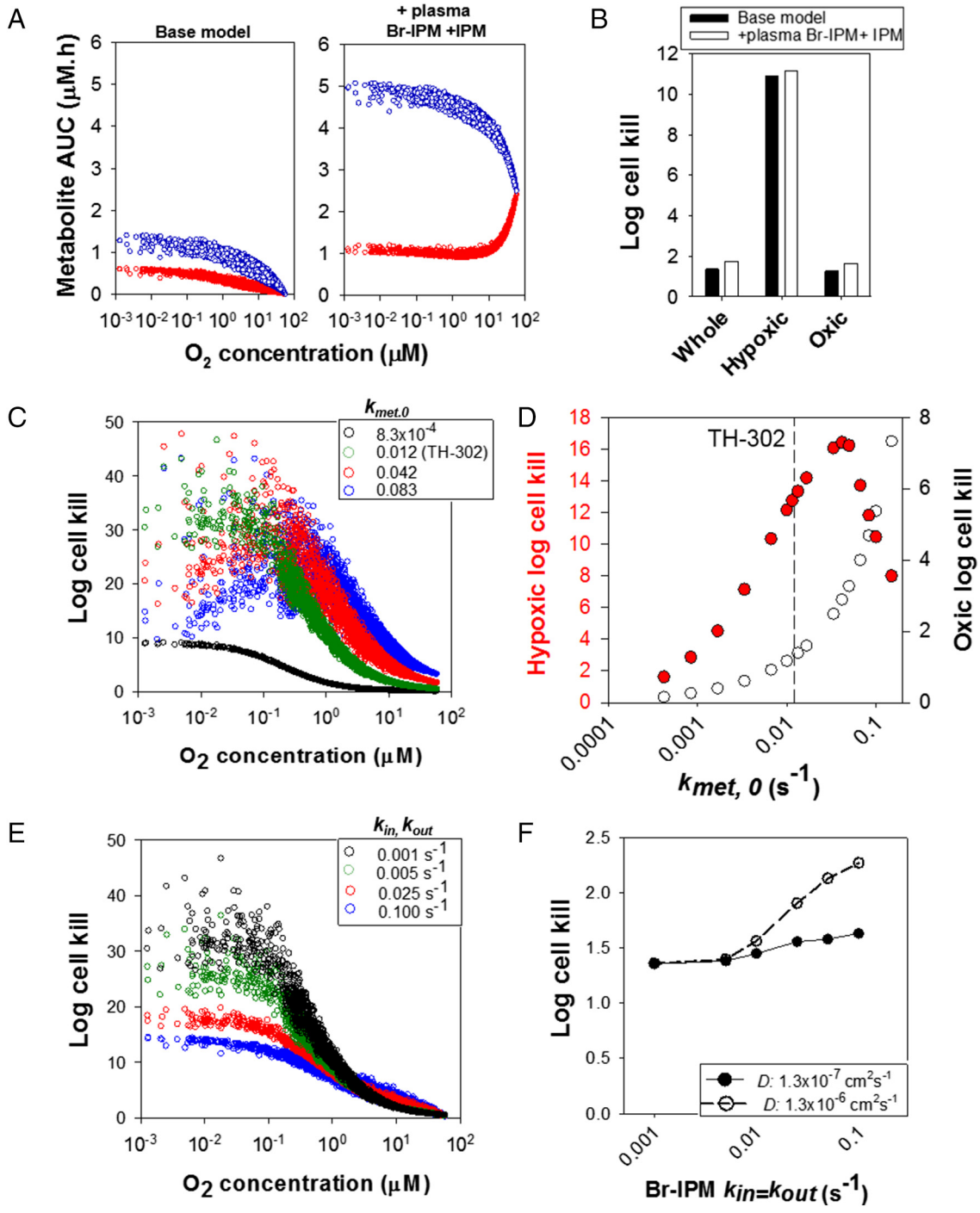

Figure 6. Modulation of the SR-PK/PD parameters from the base ('bystander') model in a virtual H460 tumor using the R3230Ac microvascular network. (A,B) Predicted extracellular AUC of Br-IPM and IPM (A) and average log cell kill in the whole tumor microregion or hypoxic (O_2< 1 μM) and oxic (O_2> 1 μM) sub-regions (B) when only TH-302 AUC was used as an input to inflowing vessels (base model) or when systemic plasma Br-IPM and IPM were added (Table S1). (C,D) Effect of changing the rate constant for prodrug activation under anoxia ($k_{met,0}$). (C) Log cell kill probability across O_2 concentrations at indicated values for $k_{met,0}$. (D) Average log cell kill in hypoxic (O_2< 1 μM, left axis) and oxic regions (O_2> 1 μM, right axis). The dashed line corresponds to the $k_{met,0}$ of TH-302. (E,F) Modulation of the membrane permeability (k_{in}, k_{out}) of the cytotoxic metabolites, assuming k_{in} = k_{out} and that the values for the distal metabolite are half that of the proximal metabolite (as for Br-IPM/ IPM). (E) Log cell kill probability across O_2 concentrations at indicated k_{in}, k_{out} of the proximal metabolite. (F) Average log cell kill across a range of membrane permeability rate constants for the proximal metabolite with diffusion coefficient of the metabolites (D) the same as Br-IPM/ IPM or 10-fold higher.

and its major metabolites in multicellular tumor models. Further, we use these parameters to calculate exposure to TH-302 and its metabolites, and the probability of cell killing, as a function of location within tumor microenvironments. The tumors we consider are virtual in the sense that they are in silico constructs generated by populating real microvascular networks, for which blood flows have

been measured, with tumor cells for which TH-302 metabolism and cell killing has been determined.

The SR-PK/PD models build on our recent demonstration that both Br-IPM and IPM are effectively cell entrapped [33]. Although IPM, generated spontaneously from Br-IPM in culture medium, diffuses across MCLs effectively (Figure 3, *A* and *B*), the SR-PK/PD models show that including the limited transport of these largely cell entrapped metabolites has almost no effect on model predictions. We demonstrate this lack of a significant bystander effect in two microvascular networks that have distinctly different features, with greater killing of hypoxic cells in the FaDu network. We conclude that Br-IPM does not generate bystander effects from TH-302 as has been supposed [23,26,31].

These findings do not preclude the possibility that the hydroxylamino metabolite of TH-302 (**1**) generates a bystander effect. The latter has a higher calculated $LogD_{7.4}$ than Br-IPM or IPM (0.29 versus −2.21 and– 2.64 respectively [33]), and clearly diffuses out of MCLs when generated by NfsA-mediated reduction of TH-302 (Figure 3, *C* and *D*) although it was not possible to quantify this because authentic **1** is not synthetically accessible. Thus **1** could diffuse to adjoining cells and then fragment to release Br-IPM. However, we note that metabolite **2** appears to be much more abundant than **1** (Figure 3, *E* and *F*). Cmpd **2** has been suggested to result from hydration of the C4-C5 double bond in **1** resulting in stabilization against fragmentation to Br-IPM [33], which would compete with formation of Br-IP. In addition, reduction to **1** and **2** by oxygen-inhibited one-electron reductases in tumor cells is much less prominent than by NfsA (Figure 3, *C*–*F*) because fragmentation of the nitro radical competes with its further reduction [33].

While we cannot rigorously exclude a role for the hydroxylamine, the important finding from the SR-PK/PD modeling is that there is no need to invoke a bystander effect to account for the monotherapy activity of TH-302 — at least in H460 tumors for which clonogenic cell killing has been quantified following a single TH-302 dose [26]. Our modeling indicates not only that a bystander effect is not required, but clarifies why TH-302 is able to kill "oxic" cells in tumors. Specifically, the very high plasma AUC achievable in mice (25 μM.h after i.v. TH-302 at 50 mg/kg, [46]) ensures that concentrations are sufficient to provide significant bioreductive activation despite partial inhibition by O_2. We note that the plasma PK used in the present model is in the range reported in humans [20], so is relevant to clinical studies with TH-302. We also note the correlation between monotherapy tumor growth delay by TH-302, following multiple doses, and pretreatment pimonidazole hypoxic fraction for a panel of 11 xenografts [26]. Those data are not readily amenable to modeling given that the hypoxic fraction, and other determinants of TH-302 sensitivity, will change during treatment. However, the observed correlation is not inconsistent with our models given that tumors with high hypoxic fraction are also expected to contain many cells able to significantly bioactivate TH-302 even if they are not sufficiently hypoxic for detectable pimonidazole binding.

The finding that the SR-PK/PD model is broadly in agreement with measured TH-302 monotherapy cell killing in H460 tumors, and with the changes observed when respiratory O_2 concentrations are altered (Figure 5) encouraged us to use the model to explore aspects of the pharmacology of TH-302 that would be difficult to investigate experimentally. We show that circulating Br-IPM (and potentially IPM, which has not been measured) is likely to make little contribution to monotherapy activity of TH-302, consistent with evidence that a very high plasma AUC of IPM (~ 100 μM.h) is required to elicit antitumor activity [49–51]. However, more information would be needed about the plasma PK of Br-IPM and its downstream metabolites in humans and rodents to assess this fully. Given that TH-302 penetration into hypoxic tissue is limited by its metabolic consumption (Figure 4, *A*–*C*), as for other classes of HAPs [35,43], we also varied $k_{met,0}$ in the base model to investigate whether the measured rates in HCT116 and H460 cells are optimal for tumor activity. This suggested that an analogue with a 4-fold higher rate of bioreductive metabolism would achieve slightly greater tumor cell killing in the hypoxic compartment of H460 or HCT116 tumors (Figure 6*D*). However faster kinetics of one-electron metabolism could come at the cost of increased normal tissue toxicity as implied in Figure 6*D* by the increased cytotoxicity against oxic tumor cells and consequent decrease in hypoxia dependence at high $k_{met,0}$. It was also instructive to model release of cytotoxins with higher membrane permeability than Br-IPM and IPM (Figure 6*F*); this increased cell killing averaged over the whole network although achieving a worthwhile increase in bystander efficiency would also require metabolites with higher tissue diffusion coefficients. Both could potentially be achieved with more lipophilic alkylating agents, as we have illustrated recently with the dinitrobenzamide mustard HAP PR-104A which generates DNA-crosslinking metabolites with $LogD_{7.4}$ values up to 1.45 [52]. However, we note that optimization of a TH-302-like HAP would play out slightly differently in a combined modality rather than monotherapy setting where the critical target population is defined by cells that are spared by the second agent.

In conclusion, SR-PK/PD modeling confirms that TH-302 is highly effective in selectively targeting hypoxic cells in tumors, as demonstrated in preclinical studies. It also demonstrates that the single agent activity of TH-302, which requires killing of relatively well-oxygenated cells that drive tumor growth, reflects the high concentrations achievable in these cells because of the favorable systemic (plasma) PK of this well-tolerated HAP. Notably, a bystander effect is not required to account for this antitumor activity. The ideal HAP for exploiting tumor hypoxia might combine the systemic PK and toxicology of TH-302 with release of a cytotoxin that has a greater ability to diffuse from hypoxic cells. Although that would increase loss into the systemic circulation, SR-PK/PD modeling of normal tissue and tumor microvascular networks [19] has demonstrated that washout of high-permeability metabolites from well-vascularized normal tissue can enhance overall selectivity for hypoxic tumor cells.

Author Contributions

C.H. performed the experiments and analyzed the data; K.H. developed the computational tools; C.H., W.W., and K.H. contributed to the design of the research and wrote the manuscript.

Acknowledgements

We thank Dr. Charles Hart (Threshold Pharmaceuticals) for providing TH-302 and Br-IPM, and for valuable comments on the manuscript, Dr. Benjamin Dickson for providing the stable isotope internal standards for LC–MS/MS, Dr. Gib Bogle for assistance with the monolayer metabolism model and Professor Timothy Secomb for assistance with the Green's function model.

Appendix A. Supplementary data

Supplementary data to this article can be found online at https://doi.org/10.1016/j.neo.2018.11.009.

References

[1] Eales KL, Hollinshead KER, and Tennant DA (2016). Hypoxia and metabolic adaptation of cancer cells. *Oncogene* **5**, e190. https://doi.org/10.1038/oncsis.2015.50.

[2] Nakazawa MS, Keith B, and Simon MC (2016). Oxygen availability and metabolic adaptations. *Nat Rev Cancer* **16**, 663–673. https://doi.org/10.1038/nrc.2016.84.

[3] Chouaib S, Noman MZ, Kosmatopoulos K, and Curran MA (2016). Hypoxic stress: obstacles and opportunities for innovative immunotherapy of cancer. *Oncogene* **36**, 439–445. https://doi.org/10.1038/onc.2016.225.

[4] Phillips RM (2016). Targeting the hypoxic fraction of tumours using hypoxia-activated prodrugs. *Cancer Chemother Pharmacol* **77**, 441–457. https://doi.org/10.1007/s00280-015-2920-7.

[5] Harris AL (2002). Hypoxia – a key regulatory factor in tumour growth. *Nat Rev Cancer* **2**, 38–47.

[6] Nordsmark M, Bentzen SM, Rudat V, Brizel D, Lartigau E, Stadler P, Becker A, Adam M, Molls M, and Dunst J, et al (2005). Prognostic value of tumor oxygenation in 397 head and neck tumors after primary radiation therapy. An international multi-center study. *Radiother Oncol* **77**, 18–24.

[7] Brizel DM, Dodge RK, Clough RW, and Dewhirst MW (1999). Oxygenation of head and neck cancer: changes during radiotherapy and impact on treatment outcome. *Radiother Oncol* **53**, 113–117.

[8] Hockel M, Schlenger K, Aral B, Mitze M, Schaffer U, and Vaupel P (1996). Association between tumor hypoxia and malignant progression in advanced cancer of the uterine cervix. *Cancer Res* **56**, 4509–4515.

[9] Horsman MR and Overgaard J (2016). The impact of hypoxia and its modification of the outcome of radiotherapy. *J Radiat Res* (Suppl. 1), i90–i98. https://doi.org/10.1093/jrr/rrw007.

[10] Brown JM and Wilson WR (2004). Exploiting tumor hypoxia in cancer treatment. *Nat Rev Cancer* **4**, 437–447.

[11] Baran N and Konopleva M (2017). Molecular pathways: hypoxia-activated prodrugs in cancer therapy. *Clin Cancer Res* **23**, 2382–2390. https://doi.org/10.1158/1078-0432.CCR-16-0895.

[12] Wilson WR and Hay MP (2011). Targeting hypoxia in cancer therapy. *Nat Rev Cancer* **11**, 393–410. https://doi.org/10.1038/nrc3064.

[13] Guise CP, Abbattista MR, Tipparaju SR, Lambie NK, Su J, Li D, Wilson WR, Dachs GU, and Patterson AV (2012). Diflavin oxidoreductases activate the bioreductive prodrug PR-104A under hypoxia. *Mol Pharmacol* **81**, 31–40. https://doi.org/10.1124/mol.111.073759.

[14] Hunter FW, Young RJ, Shalev Z, Vellanki RN, Wang J, Gu Y, Joshi N, Sreebavan S, Weinreb I, and Goldstein DP, et al (2015). Identification of P450 oxidoreductase as a major determinant of sensitivity to hypoxia-activated prodrugs. *Cancer Res* **75**, 4211–4223. https://doi.org/10.1158/0008-5472.CAN-15-1107.

[15] Hunter FW, Wouters BG, and Wilson WR (2016). Hypoxia-activated prodrugs: paths forward in the era of personalised medicine. *Br J Cancer* **114**, 1071–1077. https://doi.org/10.1038/bjc.2016.79.

[16] Wilson WR, Hicks KO, Pullen SM, Ferry DM, Helsby NA, and Patterson AV (2007). Bystander effects of bioreductive drugs: potential for exploiting pathological tumor hypoxia with dinitrobenzamide mustards. *Radiat Res* **167**, 625–636.

[17] Wilson WR, Pullen SM, Hogg A, Helsby NA, Hicks KO, and Denny WA (2002). Quantitation of bystander effects in nitroreductase suicide gene therapy using three-dimensional cell cultures. *Cancer Res* **62**, 1425–1432.

[18] Foehrenbacher A, Patel K, Abbattista M, Guise CP, Secomb TW, Wilson WR, and Hicks KO (2013). The role of bystander effects in the antitumor activity of the hypoxia-activated prodrug PR-104. *Front Oncol* **3**, 263. https://doi.org/10.3389/fonc.2013.00263.

[19] Foehrenbacher A, Secomb TW, Wilson WR, and Hicks KO (2013). Design of optimized hypoxia-activated prodrugs using pharmacokinetic/pharmacodynamic modeling. *Front Oncol* **3**314. https://doi.org/10.3389/fonc.2013.00314.

[20] Weiss GJ, Infante JR, Chiorean EG, Borad MJ, Bendell JC, and Molina JR, et al (2011). Phase 1 study of the safety, tolerability, and pharmacokinetics of TH-302, a hypoxia-activated prodrug, in patients with advanced solid malignancies. *Clin Cancer Res* **17**, 2997–3004. https://doi.org/10.1158/1078-0432.CCR-10-3425.

[21] Borad MJ, Reddy SG, Bahary N, Uronis HE, Sigal D, Cohn AL, Schelman WR, Stephenson Jr J, Chiorean EG, and Rosen PJ (2014). Randomized phase II trial of gemcitabine plus TH-302 versus gemcitabine in patients with advanced pancreatic cancer. *J Clin Oncol* **33**, 1475–1481.

[22] Chawla SP, Cranmer LD, Van Tine BA, Reed DR, Okuno SH, Butrynski JE, Adkins DR, Hendifar AE, Kroll S, and Ganjoo KN (2014). Phase II study of the safety and antitumor activity of the hypoxia-activated prodrug TH-302 in combination with doxorubicin in patients with advanced soft tissue sarcoma. *J Clin Oncol* **32**, 3299–3306.

[23] Saggar JK and Tannock IF (2014). Activity of the hypoxia-activated pro-drug TH-302 in hypoxic and perivascular regions of solid tumors and its potential to enhance therapeutic effects of chemotherapy. *Int J Cancer* **134**, 2726–2734. https://doi.org/10.1002/ijc.28595.

[24] Zhang L, Marrano P, Wu B, Kumar S, Thorner P, and Baruchel S (2016). Combined antitumor therapy with metronomic topotecan and hypoxia-activated prodrug, evofosfamide, in neuroblastoma and rhabdomyosarcoma preclinical models. *Clin Cancer Res* **22**, 2697–2708. https://doi.org/10.1158/1078-0432.CCR-15-1853.

[25] Duran R, Mirpour S, Pekurovsky V, Ganapathy-Kanniappan S, Brayton CF, Cornish TC, Gorodetski B, Reyes J, Chapiro J, and Schernthaner RE (2016). Preclinical Benefit of Hypoxia-Activated Intra-arterial Therapy with Evofosfamide in Liver Cancer. *Clin Cancer Res* **23**, 536–548. https://doi.org/10.1158/1078-0432.CCR-16-0725.

[26] Sun JD, Liu Q, Wang J, Ahluwalia D, Ferraro D, Wang Y, Duan JX, Ammons WS, Curd JG, and Matteucci MD, et al (2012). Selective tumor hypoxia targeting by hypoxia-activated prodrug TH-302 inhibits tumor growth in preclinical models of cancer. *Clin Cancer Res* **18**, 758–770. https://doi.org/10.1158/1078-0432.CCR-11-1980.

[27] Sun JD, Liu Q, Ahluwalia D, Ferraro DJ, Wang Y, Jung D, Matteucci MD, and Hart CP (2016). Comparison of hypoxia-activated prodrug evofosfamide (TH-302) and ifosfamide in preclinical non-small cell lung cancer models. *Cancer Biol Ther* , 1–10. https://doi.org/10.1080/15384047.2016.1139268.

[28] Duan JX, Jiao H, Kaizerman J, Stanton T, Evans JW, Lan L, Lorente G, Banica M, Jung D, and Wang J, et al (2008). Potent and highly selective hypoxia-activated achiral phosphoramidate mustards as anticancer drugs. *J Med Chem* **51**, 2412–2420. https://doi.org/10.1021/jm701028q.

[29] Meng F, Evans JW, Bhupathi D, Banica M, Lan L, Lorente G, Duan JX, Cai X, Mowday AM, and Guise CP, et al (2012). Molecular and cellular pharmacology of the hypoxia-activated prodrug TH-302. *Mol Cancer Ther* **11**, 740–751. https://doi.org/10.1158/1535-7163.MCT-11-0634.

[30] Anderson RF, Li D, and Hunter FW (2017). Antagonism in effectiveness of evofosfamide and doxorubicin through intermolecular electron transfer. *Free Radic Biol Med* **113**, 564–570. https://doi.org/10.1016/j.freeradbiomed.2017.10.385.

[31] Hajj C, Russell J, Hart CP, Goodman KA, Lowery MA, Haimovitz-Friedman A, Deasy JO, and Humm JL (2017). A combination of radiation and the hypoxia-activated prodrug evofosfamide (TH-302) is efficacious against a human orthotopic pancreatic tumor model. *Transl Oncol* **10**, 760–765. https://doi.org/10.1016/j.tranon.2017.06.010.

[32] Olive PL and Banaíth JP (2009). Kinetics of H2AX phosphorylation after exposure to cisplatin. *Cytometry B Clin Cytom* **76**, 79–90. https://doi.org/10.1002/cyto.b.20450.

[33] Hong CR, Dickson B, Jaiswal J, Pruijn FB, Hunter FW, Hay MP, Hicks KO, and Wilson WR (2018). Cellular pharmacology of evofosfamide (TH-302): a critical re-evaluation of its bystander effects. *Biochem Pharmacol* **156**, 265–280. https://doi.org/10.1016/j.bcp.2018.08.027.

[34] Hicks KO, Siim BG, Jaiswal JK, Pruijn FB, Fraser AM, Patel R, Hogg A, Liyanage HDS, Dorie MJ, and Brown JM, et al (2010). Pharmacokinetic/pharmacodynamic modeling identifies SN30000 and SN29751 as tirapazamine analogues with improved tissue penetration and hypoxic cell killing in tumors. *Clin Cancer Res* **16**, 4946–4957. https://doi.org/10.1158/1078-0432.CCR-10-1439.

[35] Hicks KO, Pruijn FB, Secomb TW, Hay MP, Hsu R, Brown JM, Denny WA, Dewhirst MW, and Wilson WR (2006). Use of three-dimensional tissue cultures to model extravascular transport and predict in vivo activity of hypoxia-targeted anticancer drugs. *J Natl Cancer Inst* **98**, 1118–1128.

[36] Hicks KO, Siim BG, Pruijn FB, and Wilson WR (2004). Oxygen dependence of the metabolic activation and cytotoxicity of tirapazamine: implications for extravascular transport and activity in tumors. *Radiat Res* **161**, 656–666.

[37] Hicks KO, Myint H, Patterson AV, Pruijn FB, Siim BG, Patel K, and Wilson WR (2007). Oxygen dependence and extravascular transport of hypoxia-activated prodrugs: comparison of the dinitrobenzamide mustard PR-104A and tirapazamine. *Int J Radiat Oncol Biol Phys* **69**, 560–571.

[38] Secomb TW, Hsu R, Braun RD, Ross JR, Gross JF, and Dewhirst MW (1998). Theoretical simulation of oxygen transport to tumors by three-dimensional networks of microvessels. *Adv Exp Med Biol* **454**, 629–634.

[39] Hicks KO, Pruijn FB, Baguley BC, and Wilson WR (2001). Extravascular transport of the DNA intercalator and topoisomerase poison *N*-[2-(dimethylamino)ethyl]acridine-4-carboxamide (DACA): diffusion and metabolism in multicellular layers of tumor cells. *J Pharmacol Exp Ther* **297**, 1088–1098.

[40] Wilson WR and Hicks KO (1999). Measurement of extravascular drug diffusion in multicellular layers. *Br J Cancer* **79**, 1623–1626.

[41] Hicks KO, Fleming Y, Siim BG, Koch CJ, and Wilson WR (1998). Extravascular diffusion of tirapazamine: effect of metabolic consumption assessed using the multicellular layer model. *Int J Radiat Oncol Biol Phys* **42**, 641–649.

[42] Hicks KO, Ohms SJ, van Zijl PL, Denny WA, Hunter PJ, and Wilson WR (1997). An experimental and mathematical model for the extravascular transport of a DNA intercalator in tumours. *Br J Cancer* **76**, 894–903.

[43] Hicks KO, Pruijn FB, Sturman JR, Denny WA, and Wilson WR (2003). Multicellular resistance to tirapazamine is due to restricted extravascular transport: a pharmacokinetic/pharmacodynamic study in HT29 multicellular layer cultures. *Cancer Res* **63**, 5970–5977.

[44] Prosser GA, Copp JN, Syddall SP, William EM, Smaill JB, Wilson WR, Patterson AV, and Ackerley DF (2010). Discovery and evaluation of *Escherichia coli* nitroreductases that activate the anticancer prodrug CB 1954. *Biochem Pharmacol* **79**, 678–687. https://doi.org/10.1016/j.bcp.2009.10.008.

[45] Pries AR, Cornelissen AJ, Sloot AA, Hinkeldey M, Dreher MR, Hoepfner M, Dewhirst MW, and Secomb TW (2009). Structural adaptation and heterogeneity of normal and tumor microvascular networks. *PLoS Comput Biol* **5**e1000394. https://doi.org/10.1371/journal.pcbi.1000394.

[46] Jung D, Lin L, Jiao H, Cai X, Duan JX, and Matteucci M (2012). Pharmacokinetics of TH-302: a hypoxically activated prodrug of bromo-isophosphoramide mustard in mice, rats, dogs and monkeys. *Cancer Chemother Pharmacol* **69**, 643–654. https://doi.org/10.1007/s00280-011-1741-6.

[47] Collares-Buzato CB, McEwan GT, Jepson MA, Simmons NL, and Hirst BH (1994). Paracellular barrier and junctional protein distribution depend on basolateral extracellular Ca^{2+} in cultured epithelia. *Biochim Biophys Acta* **1222**, 147–158.

[48] Peeters SG, Zegers CM, Biemans R, Lieuwes NG, van Stiphout RG, Yaromina A, Sun JD, Hart CP, Windhorst AD, and van EW, et al (2015). TH-302 in combination with radiotherapy enhances the therapeutic outcome and is associated with pretreatment [18F]HX4 hypoxia PET imaging. *Clin Cancer Res* **21**, 2984–2992.

[49] Wang JJH and Chan KK (1995). Analysis of ifosfamide, 4-hydroxyifosfamide, N2-dechloroethylifosfamide, N3-dechloroethylifosfamide and iphosphoramide mustard in plasma by gas chromatography-mass spectrometry. *J Chromatogr B Biomed Appl* **674**, 205–217.

[50] Germann N, Urien S, Rodgers AH, Ratterree M, Struck RF, Waud WR, Serota DG, Bastian G, Jursic BS, and Morgan LR (2005). Comparative preclinical toxicology and pharmacology of isophosphoramide mustard, the active metabolite of ifosfamide. *Cancer Chemother Pharmacol* **55**, 143–151.

[51] Zheng JJ, Chan KK, and Muggia F (1994). Preclinical pharmacokinetics and stability of isophosphoramide mustard. *Cancer Chemother Pharmacol* **33**, 391–398.

[52] Hong CR, Bogle G, Wang J, Patel K, Pruijn FB, Wilson WR, and Hicks KO (2018). Bystander effects of hypoxia-activated prodrugs: agent-based modelling using three dimensional cell cultures. *Front Pharmacol* **9**, 1013. https://doi.org/10.3389/fphar.2018.01013.